International Journal of Aquatic Science
ISSN: 2008-8019
Vol 12, Issue 02, 2021

Electrical and Dielectric properties of Lead Zirconate titanate [$PbZr_{0.52}Ti_{0.48}O_3$] synthesized by ceramic method.

S.P. Yadav[1], S.A. Kanade[2], Kamlesh V. Chandekar[3]

[1,3]Department of Physics, Rayat Shikshan Sanstha's, Karmaveer Bhaurao Patil College, Vashi, Navi Mumbai-400703, India
[2] Department of Physics, J.S. M. College, Alibag -402201, India.

Email: [3]kamlex_chandekar@yahoo.co.in

Abstract: ***Lead Zirconate titanate [$PbZr_{0.52}Ti_{0.48}O_3$] (PZT) material was synthesized by the ceramic route. The morphology of $PbZr_{0.52}Ti_{0.48}O_3$ sample was observed by scanning electron microscopy and its shows large grain sizes in the range of 1-4 µm. The higher dc resistivity 1.146 x10^5 (Ω.cm) was observed for PZT sample at room temperature. Temperature-dependent P-E loop measurements of PZT sample were recorded by the P-E tracer circuit. The values of remnant polarization (4.53, 2.23 and 1.28 µC/cm^2) and saturation polarization (5.60, 4.93 and 3.19 µC/cm^2) were observed at 100°C, 150 °C and 200°C respectively. The obtained coercivity values (5.14, 5.88 and 6.80 kV/cm) from the temperature-dependent P-E loops were found to be increased with an increase in the temperature. The values of dielectric constant were found between 2646 and 417 (F/cm) for PZT sample when it was exposed to the frequency of applied field varies from log (1.2) to log (6.0). The variation in loss tangent was recorded between 0.73 and 0.10 at log (3.925) and log (2.388) Hz, respectively. The frequency-dependent conductivity of PZT material was recorded at room temperature. Such types of PZT materials show good thermal stability and therefore, it can be used for high-temperature piezoelectric applications.***

Keywords: ***$PbZr_{0.52}Ti_{0.48}O_3$] (PZT), DC resistivity, P-E loop analysis, Dielectric property, AC conductivity***

1. INTRODUCTION

For many decades the researchers focusing on the ferroelectric perovskite oxides because of their various applications such as integrated memory devices, microwave devices, piezoelectric, and magneto-electric devices [1-3]. Lead zirconate titanate [$PbZr_{0.52}Ti_{0.48}O_3$] (PZT) materials based on the ferroelectric property due to their outstanding physical properties like large polarization, large piezoelectricity, and electro-optical property. The PZT ceramic material with such outstanding physical properties makes them suitable for various applications such as FRAM, sensors, oscillators, and transducers [4-9]. The excellent piezoelectric property of PZT materials makes them ideal materials for MEMS applications. These physical properties of PZT materials depend on the fluctuation and motion or vibration of domain walls (DWs) under electric field, even as enough polarization reversal is required for memory devices [10-12]. The domain wall (DW) pinning by mobile charged defects leads to improve mechanical

factor, which reduces the mechanical and dielectric losses, even as it prohibits the polarization from switching [13-15].

PZT material is being employed as a heat sensor since it has an excellent pyroelectric property which develops a potential difference between its faces on changing the temperature conditions. PZT is also ferroelectric material causing it to exhibit the spontaneous electric polarization that can be reversed according to the direction of an electric field. PZT has a perovskite crystal structure with a small Ti^{4+} or Zr^{4+} in a lattice of large divalent Pb^{2+} ions. PZT exhibits the ferroelectric $PbTiO_3$ (Tc=490°C) and antiferroelectric $PbZrO^3$ (Tc=230°C) respectively. The properties of PZT depend on the ratio of zirconium to titanium (Zr/Ti). According to the phase diagram of PZT solid solution has three representative phase regions rhombohedral, tetragonal and morphotropic phase boundary (MPB). The corresponding (Zr/Ti) mole ratio of the PZT composition was set (52/48). The electric properties at the composition (Zr/Ti =52/48) of PZT material are scarily observed in the literature [16, 17] and it is commonly being employed for various applications as the composition approaches to MPB region. PZT materials have a large dielectric constant, piezoelectric, and poling efficiency when the concentration (x) approaches 0.52. It is due to the enhanced number of admissible domain states at the morphotropic phase boundary (MPB). For the present study, we prepared PZT with Zr/Ti mole ratio (52/48) having chemical composition $PbZr_{0.52}Ti_{0.48}O_3$. In order to improve the performance in favor of specific applications, a number of studies were reported by the researchers on the doping effect of PZT-based ferroelectric ceramic [18-20].

2. EXPERIMENTAL

2.1 Synthesis of ferroelectric

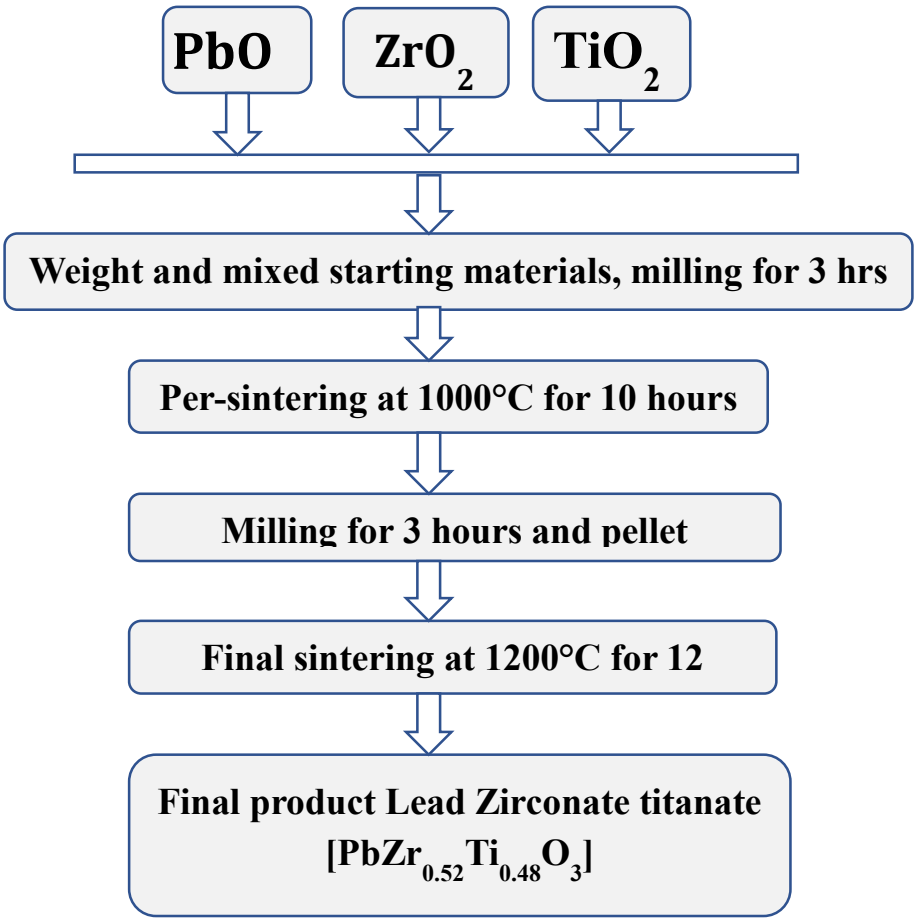

Fig. 1: Flow chart of preparation of ferroelectric ($PbZr_{0.52}Ti_{0.48}O_3$) sample

Lead Zirconate titanate [$PbZr_{0.52}Ti_{0.48}O_3$] of stoichiometric composition was prepared using (PbO, 99.9 %), (ZrO_2, 99.9 %) and (TiO_2, 99.9 %) as precursors. These chemicals were taken in stoichiometric amounts, grinded properly, and mixed in an agate mortar. The obtained mixture of these chemicals was initially heated at 1000 °C for 10 hours at the heating time of 5 °C min^{-1}. The resulting powder was again grinded in an agate mortar for 3 hours and a hydraulic press was used to make a pellet. The obtained pellets were heated at 1200 °C for 12 hours. Fig. 1 shows a flow chart of preparation for ferroelectric PZT [Pb ($Zr_{0.52}Ti_{0.48}$) O_3] by ceramics method.

$PbO + (0.52)\ ZrO_2 + (0.48)\ TiO_2 \rightarrow Pb\ Zr_{0.52}Ti_{0.48}O_3$

2.2. Characterization tools

Morphology of the $PbZr_{0.52}Ti_{0.48}O_3$ sample was obtained by using analytical SEM (Model JEOL, JSM-6360A) at 10,000 X magnification. The P-E hysteresis measurement of the PZT sample was done using the P-E loop Tracer operates at 50 Hz.

3. RESULTS AND DISCUSSION

3.1 X ray diffraction

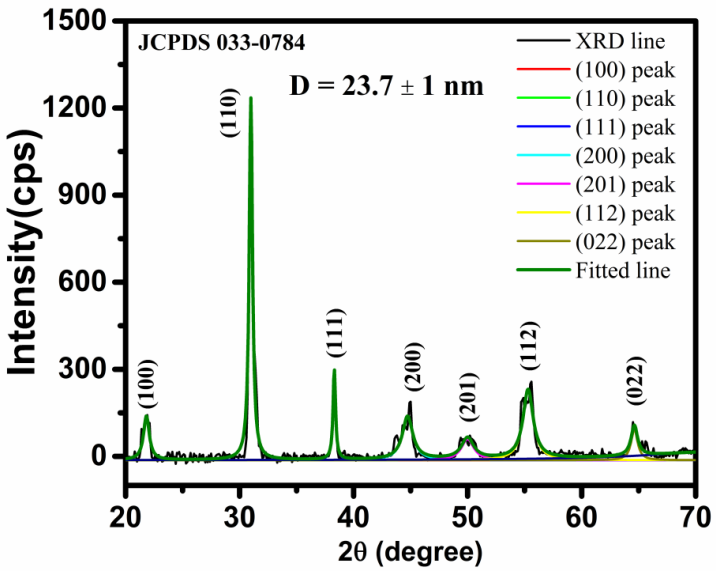

Fig. 2: Diffraction pattern of $PbZr_{0.52}Ti_{0.48}O_3$ sample is fitted using Lorentz function and obtained values of 2θ and β were used to estimate the average crystallite size of the PZT.

X-ray diffraction (XRD) pattern of $PbZr_{0.52}Ti_{0.48}O_3$ (PZT) material is exhibited in Fig. 2. All indexed peaks of the XRD pattern correspond to JCPDS card (#033-0784), which confirms the formation of the tetragonal perovskite structure of PZT material. The absence of any extra in XRD pattern confirms the formation of a single-phase structure of the PZT material. The more intense peak was observed at (110) plane which corresponds to the preferred orientation of crystallites due to the higher growth rate of the crystallites along thus plane compared to other planes. It was caused by the lowest energy of (110) plane with respect

to other planes like (100) and (111). The lattice parameters and their ratio ($c/a = 0.9919$) were estimated using the relations reported in the literature and found in good agreement with the reported values [21]. The obtained values of lattice parameters are tabulated in Table 1. The data points of the XRD was fitted using the Lorentz function and the obtained values of diffraction angle 2θ and full width at half maximum β for most intense peak (110) were reported in Table 1. The average crystallite size D was evaluated using the Debye Scherrer relation $D = 0.9\lambda/\beta\cos\theta$ by considering the obtained values of 2θ and β from the fitting profile of XRD pattern (Table 1). The lattice parameter for tetragonal perovskite structure is calculated by using the formula

$$\frac{1}{d_{hkl}^2} = \frac{h^2 + k^2}{a^2} + \frac{l^2}{c^2} \qquad (1)$$

where, the symbols have their usual meanings with condition of $a = b \neq c$.

Table 1: Data on lattice parameters (c, a) and their ratio c/a of PZT

Sample	2θ (deg.) at (110) plane	β (deg.) at (110) plane	D (nm)	a (Å)	c (Å)	c/a
$PbZr_{0.52}Ti_{0.48}O_3$	30.98757± 0.00252	0.34643± 0.00724	23.7 ±1.0	4.078	4.045	0.9919

3.2 Scanning electron microscopy

Morphology of the $PbZr_{0.52}Ti_{0.48}O_3$ sample was obtained by using analytical SEM (Model JEOL, JSM-6360A) at 10,000 X magnification. Fig.3 shows well-grown and well-connected grains. The scanning electron micrograph of PZT shows good grain growth with a larger grain size within nearly 1- 4µm.

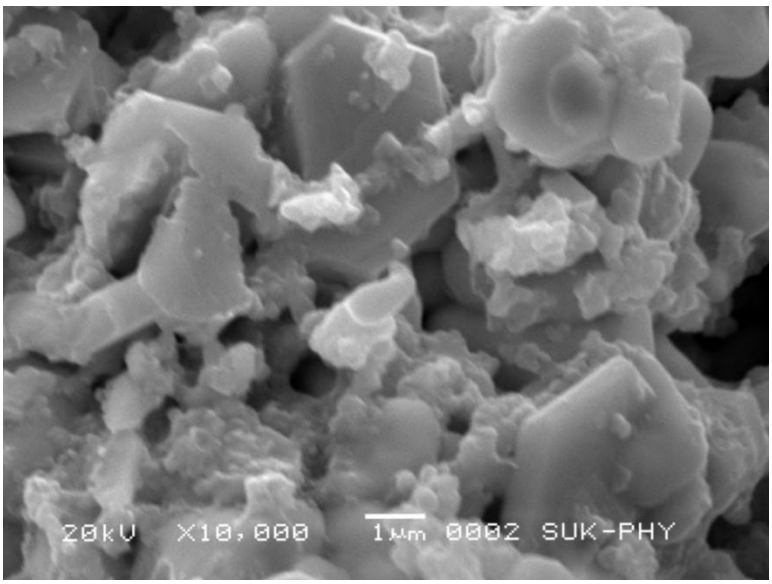

Fig. 3: Scanning electron microscopy of image of $PbZr_{0.52}Ti_{0.48}O_3$ (PZT) sample.

3.3 Electrical Properties
3.3.1 DC electrical resistivity

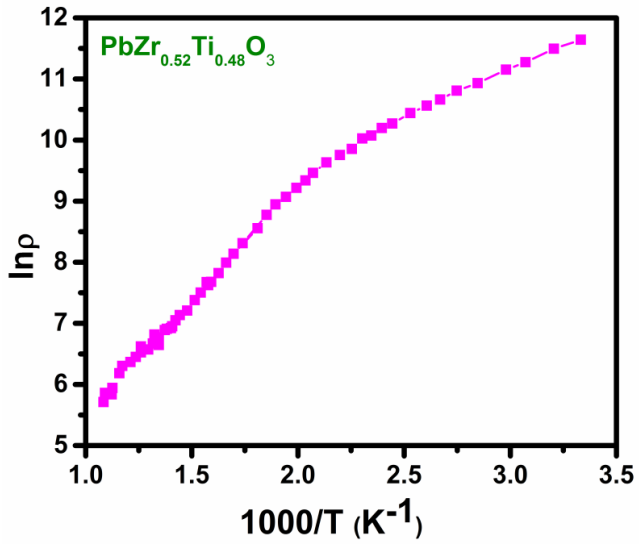

Fig. 4: Variation of dc resistivity with temperature for $PbZr_{0.52}Ti_{0.48}O_3$ sample

The existence of free and localized charge carriers can be investigated using the variation of electrical resistivity with the temperature. Fig. 4 exhibits the variations of DC electrical resistivity ρ_{dc} within the temperature varies from RT to 700 K. From the plot, it is observed that PZT material exhibiting the semiconductor characteristics since the decrease in electric resistivity of as-prepared PZT sample with an increase in the temperature. Verwey–de Boer mechanism usually explains the electrical resistivity where inter-change of electrons occurs between the ions of the constituting elements present in more than one valence state. The presence of such ions in the material is randomly distributed over equivalent crystallographic lattice sites [22]. The drift velocity of the electrons plays a major role to decrease the resistivity of the material. In the present PZT sample, the decrease in resistivity with the temperature was observed from Fig.4. It was due to the increase in the mobility of charge carriers, which increases the concentration of free charge carriers available for conduction. Furthermore, the conduction mechanism of PZT can be explained by the hopping of electrons between Ti^{3+}/Ti^{4+}, Pb^{2+}/Pb^{3+} and Zr^{3+}/Zr^{4+} [23] i e. the electron transfer between the ions of the same material present in different electronic states. For PZT the conduction process is possibly given by the following relations.

$$Zr^{3+} \leftrightarrow Zr^{4+}$$
$$Pb^{2+} \leftrightarrow Pb^{3+}$$
$$Ti^{4+} \leftrightarrow Ti^{3+}$$

The plot of dc electrical resistivity with the temperature has been fitted using Arrhenius relation $\rho = \rho_o exp(\Delta E/kT)$ and obtained slope from the linearly fitted straight line was used to calculate the activation energy ΔE of the sample and it is found to be 0.32 eV. In the PZT ceramic, the cation to anion ratio departs from the ideal value and the oxygen vacancies may be created in as-prepared sample. These oxygen vacancies can provide trapped electrons to give raise to n-type of conductivity. Similarly, p-type conductivity has also been reported by Patil and Lokare et al. [24, 25]. The change in slope is observed nearly at 450 K (transition temperature) and is due to the phase transition from a ferroelectric to a paraelectric state.

3.3.2 P-E Loop measurement

The variation of polarisation with applied dc electric field was recorded by polarization-electric (P-E) loop tracer at RT and showed in Fig. 5 (a).

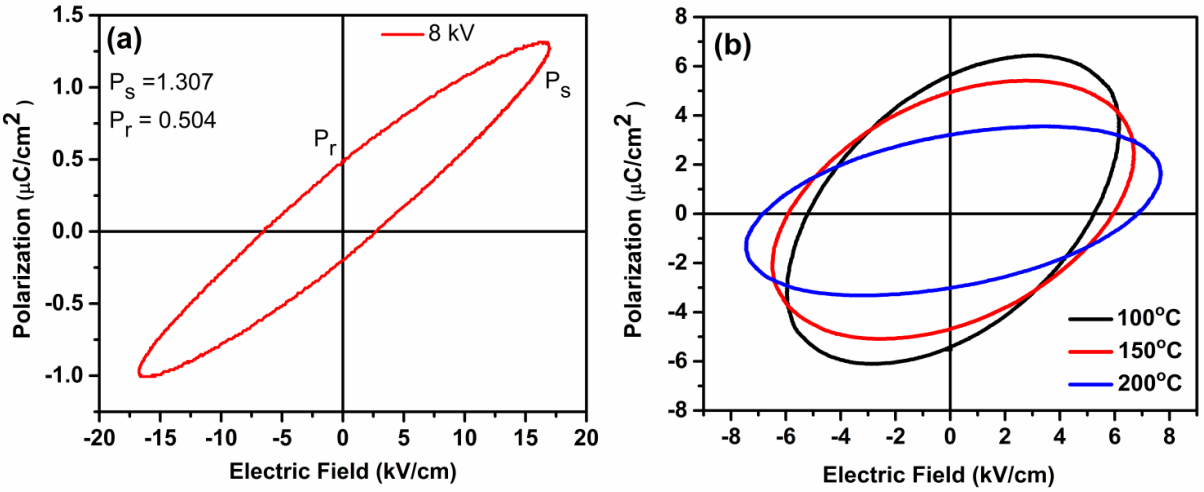

Fig. 5: (a) P-E loop at room temperature and (b) Temperature-dependent P-E loop analysis of $PbZr_{0.52}Ti_{0.48}O_3$ sample

The non-zero remnant polarisation was observed at zero electric fields and the ability to reverse the direction of polarisation with the direction of the electric field. Furthermore, the temperature-dependent P-E analysis was also recorded for the present PZT sample. Fig. 5 (b) shows P-E hysteresis plots for PZT at temperatures 100, 150, and 200°C respectively. From the measurements of all P-E loop parameters (Ec, Ps, and Pr), it is confirmed that the PZT material exhibiting the ferroelectric property. A comparison of P-E loops reveals that both the remnant polarization (Pr) and saturation polarization (Ps) decrease with an increase in the temperature of PZT material (Fig. 5b). It is also concluded that the ferroelectric property of the PZT material becoming weak with an increase in temperature. The reduction in the ferroelectric behaviour of the PZT material with the temperature may be due to the distribution of charge causing the shape of the P-E loop to distort from its normal shape with the application of an external electric field. The obtained values of Ec, Ps, Pr, and their (Pr/Ps) are tabulated in Table 2, where it is found that the obtained values of Ps and Pr of P-E loops decrease with an increase in the temperature. But, the values of coercivity (Ec) and (Pr/Ps) of P-E loops increase with the temperature was observed from Fig. 5(b). From table 2, it can be seen that there is an increase in the (Pr/Ps) with temperature which indicates a decrease in the homogeneity and uniformity

of grains with the temperature [26]. The temperature-dependent P-E loop becomes attenuate with an increase in the temperature, denoting the improvement from normal ferroelectric to relaxor ferroelectric, which exhibits a high value of electrostriction at higher temperatures. The temperature-dependent P-E loop becomes attenuate and their values Ps and Pr tend to decrease under an applied electric field. Such type of phenomenon occurred in the materials is due to the increase of Ec rather than a decrease of the long-range interaction of dipoles on cooling, and therefore, they do not express the re-entrant relaxor behaviour. The decrease in the long-range ordered behaviour of electric dipoles in the ferroelectric phase results in the low internal polarizability of the ferroelectric material [18]. The ferroelectric property of PZT material can be employed in information storage devices like non-volatile RAM.

Table 2: Polarization measurement of ferroelectric ($PbZr_{0.52}Ti_{0.48}O_3$)

Temperature	Coercivity (Ec) (kV/cm)	Saturation polarization (Ps) ($\mu C/cm^2$)	Remnant polarization (Pr) ($\mu C/cm^2$)	Squareness ratio (Pr /Ps)
100°C	5.14	5.60	4.53	1.23
150°C	5.88	4.93	2.23	2.21
200°C	6.80	3.19	1.28	2.49

3.4 Dielectric properties

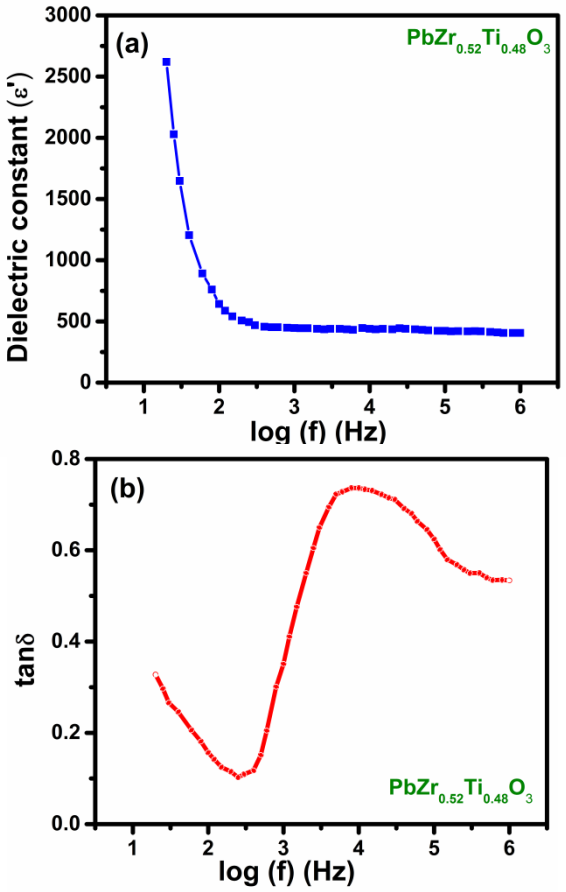

Fig. 6: (a) Variation of dielectric constant and (b) loss tangent with the frequency for $PbZr_{0.52}Ti_{0.48}O_3$ sample

Fig.6 (a) exhibits the variation of dielectric constant (ε') with the frequency. The reduction in (ε') at the lower frequencies is attributed to the dominance of the space charge (interfacial) polarization over the other polarizations like dipolar, ionic, and electronic polarization. The space charge polarization at the lower frequencies is due to the existence of the space charge effect. But, it exhibits the frequency-independent dielectric constant at the higher frequencies due to the dielectric dispersion [27]. The dielectric constant ε' is given by the Eq. (2).

$$\varepsilon' = \frac{Cd}{\varepsilon_o A} \qquad (2)$$

The reduction in (ε') with the frequency can be elaborated on the basis of Koops-phenomenological theory [27] which employs the dielectric consists of the non-homogeneous medium of two layers of the Maxwell–Wagner type [24, 25]. It is observed that the small dispersion in dielectric constants with the log (f) up to 3kHz and then after no further increase in dielectric constants with an increase in frequency because the existence of electrical diploe in the materials fails to follow the frequency of the electric field.

It is well known that the loss tangent $\tan\delta = \varepsilon''/\varepsilon'$, which corresponds to the ratio of the energy lost to the energy stored in a field. Fig. 6(b) shows the plot of the loss tangent vs log (f) for the PZT material. The dielectric loss follows a dispersion behaviour resembling the dielectric constant with frequency. Unlike ferrites, the dielectric loss is very small. This is obvious as polarization is an inherent property of the PZT ferroelectric phase. It is seen that at lower frequencies (up to log 2.5) dielectric loss decreases. Then further dielectric loss increases with increase in the frequencies. The relatively small dielectric losses are observed at lower frequencies and this may be the result of space charge polarization and also inhomogeneity in the structure. Moreover, in order to study the conduction mechanism of as-prepared PZT sample, the ac conductivity σ_{ac} of the PZT sample was carried out with the frequency (Fig. 7) and it is correlated with the dielectric constant of the material from Eq. (3).

$$\sigma_{ac} = \varepsilon' \varepsilon_o \omega \tan\delta \qquad (3)$$

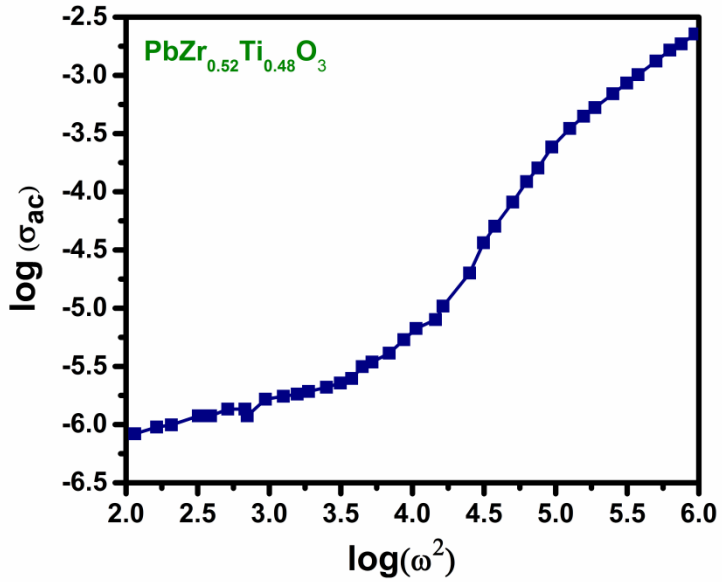

Fig. 7: Variation of ac conductivity with the frequency for $PbZr_{0.52}Ti_{0.48}O_3$ sample.

It was observed that the σ_{ac} increases with the frequency. The frequency-dependent ac conductivity was observed in Fig. 7 corresponds to the hopping mechanism of charge carriers; thereby enhancing the conductivity with the frequency. The increase in σ_{ac} with frequency can be explained on the basis of the Koops model [27, 28]. According to this model, lower conductivity was observed for PZT material at the lower frequencies. It may be due to the creation of potential barriers at the grain boundaries, which prohibits the migration of charge carriers from one grain to others, results in the reduction in the hopping mechanism, which provides the decrease in conductivity at lower frequencies. Such type of behaviour of charge carriers is attributed to the Maxwell–Wagner model.

4. CONCLUSIONS

Fine particles of ferroelectrics composition $PbZr_{0.52}Ti_{0.48}O_3$ was successfully synthesized by the ceramic method. X-ray diffraction pattern shows well-defined peaks and the more intense peak (1 1 0) confirms tetragonal perovskite structure. SEM shows good grain growth with a larger grain size within nearly 1- 4µm. The linear variation in dc electrical resistivity with temperature confirms the semiconducting nature of the samples. The activation energy in the present case is found to be 0.32 eV. PE loop measurements confirmed that the material is a ferroelectric material and polarization ratio (Pr/Ps) shows ferroelectrics behaviour is weakening with the temperature. The dielectric constant is found to decrease with an increase in frequency. Due to outstanding physical properties of PZT materials can be employed in high temperature piezoelectric applications.

Acknowledgements
Authors thankful to the Electro-chemical laboratory of Dr. K.Y. Rajpure of the Department of Physics, Shivaji University, Kolhapur.

5. REFERENCES

[1] M. Li, Z. Zhou, M. Liu, J. Lou, D. E. Oates, G. F. Dionne, M. L. Wang, N. X. Sun, J. Phys. D: Appl. Phys., 46 (2013) 275001
[2] M. Jain, N. K. Karan, R. S. Katiyar, A. S. Bhalla, F. A. Miranda, F. W. V. Keuls, Appl. Phys. Lett. 85 (2004) 275
[3] Y. Wang, H. Yu, M. Zeng, J.G.Wan, M.F. Zhang, J.M. Liu, C.W. Nan, Appl. Phys. A: Mater. Sci. Process. 81 (2005) 1197
[4] W. Lee, H. Han, A. Lotnyk, M.A. Schubert, S. Senz, M. Alexe, D. Hesse, S. Balk, U. Gosele, Nat. Nanotechnol. 3 (2008) 402
[5] M. Prabu, I.B. Shameem Banu, S. Gobalakrishnan, M. Chavali, J. Nanosci. Nanotechnol. 13(2013) 1938.
[6] Umar, Y.-B. Hahn (eds.), Metal Oxide Nanostructures and Their Applications, vol. 1–5 , American Scientific Publishers, Los Angeles, 2010.
[7] M.S. Zarnik, D. Belavic, S. Macek, J. Holc, Int. J. Appl. Ceram. Technol. 6 (2009) 9
[8] H.S. Nalwa (ed.), Encyclopedia of Nanoscience and Nanotechnology, Vol. 1–25 American Scientific Publishers, Los Angeles, 2011.
[9] .K. Min, K.-H. Kwon, J. Nanosci. Nanotechnol. 12 (2012) 6011
[10] M. F. Zhang, Y. Wang, K. F. Wang, J. S. Zhu and J.-M. Liu , J. Appl. Phys. 105 (2009) 061639
[11] N. Zhang, Z. Xu, Y. Feng, Xi Yao, J Electroceram, 21 (2008) 609
[12] V. R. Mastelaro, A. Mesquita, P. P. Neves, A. Michalowicz, M. Bounif,P S. Pizani, M. R. Joya and J. A. Eiras, J. Appl. Phys. 105 (2009) 033508
[13] M. Adamczyk, Z. Ujma, J. Hańderek, J. Appl. Phys. 89 (2001) 542
[14] D. C. Lupascu, E. Aulbach , J. Rödel, J. Appl. Phys. 93(2003) 5551
[15] T. B. Xu, E. J. Siochi, J. H. Kang, L. Zuo, W. Zhou, X. Tang, X. Jiang, Smart Mater. Struct. 22 (2013) 065015
[16] M. Prabu, I.B. Shameem Banu, S. Gobalakrishnan, M. Chavali, J. Alloys Comp. 551(2013) 200.
[17] K. Bouayad, S. Sayouri, T. Lamcharfil, M. Ezzejari, D. Mezzane, L. Hajji, A.E.I. Ghazouali, M. Filalil, P. Dieudonne, M. Rhouta, Phys. A 358 (2005)175.
[18] J. M. Liu, Y. Wang, C. Zhu, G. L. Yuan , S. T. Zhang, Appl. Phys. Lett. 87 (2005) 042904
[19] Y. Wang, Q. Shao, J. M. Liu Appl. Phys. Lett,. 88 (2006) 122902
[20] S. Priya, K. Uchino, J. Appl. Phys,. 91(2002) 4515
[21] R. S. Devan, Y. D. Kolekar, B. K. Chougule, J. Phys.: Condens. Matter 18 (2006) 9809
[22] P. A. Jadhav, M. B. Shelar, S. S. Chougule, B. K. Chougule, Physica B. 405 (2010) 857
[23] O. M. Prakash, K. D. Mandal , C. C. Christopher, M. S. Sastry, D. Kumar, Bull. Mater. Sci., 17(1994) 253
[24] D.R. Patil, S.A. Lokare, R.S. Devan, S.S. Chougule, Y.D. Kolekar, B.K. Chougule, J. Phy. Chem. Solid, 68 (2007) 1522
[25] S. A. Lokare, D. R. Patil, R. S. Devan, S. S. Chougule, Y. D. Kolekar, B. K. Chougule, Mater. Res. Bull., 43 (2008) 326
[26] K. Carl and K.H. Hardtl, Ferroelectrics 17 (1978) 473
[27] C. G. Koops, Phys. Rev. 83 (1951)127
[28] R. G. Kharabe, R. S. Devan, C. M. Kanamadi, B. K. Chougule, Smart Mater. Struct. 15 (2006) N36